

Climatic regulation of atmospheric mercury deposition: Evidence from mercury isotopes in an alpine peat core

Wen Xue^{1,2}, Runsheng Yin^{2,*}, Sae Yun Kwon³, Haijun Peng⁴, Di Chen², Mengxiu Zeng⁵, and Linchuan Fang^{1,*}

¹College of Natural Resources and Environment, Northwest A&F University, 712100 Yangling, China

²State Key Laboratory of Ore Deposit Geochemistry, Institute of Geochemistry, Chinese Academy of Sciences, 550081 Guiyang, China

³Division of Environmental Science and Engineering, Pohang University of Science and Technology, 77 Cheongam-Ro, Nam Gu, Pohang 37673, South Korea

⁴State Key Laboratory of Environmental Geochemistry, Institute of Geochemistry, Chinese Academy of Sciences, 550081 Guiyang, China

⁵College of Geography and Environmental Sciences, Zhejiang Normal University, 321004 Jinhua, China

ABSTRACT

Mercury is a global pollutant that can undergo long-range transport in the atmosphere. While anthropogenic activities have largely increased atmospheric Hg emission and deposition since global industrialization, mechanisms governing the atmospheric Hg cycle in pre-industrial periods remain unclear. Alpine peatlands receive Hg mainly from atmospheric Hg deposition and are sensitive to climatic changes, therefore alpine peat cores can be a useful archive for understanding the relationship between atmospheric Hg deposition and climate change. Here we reconstruct a 1200-year Hg deposition record based on a core drilled from an ombrotrophic peat bog in Yunnan-Guizhou Plateau, SW China. This core shows a dramatic change of Hg deposition fluxes (30.3–515 $\mu\text{g}/\text{m}^2/\text{yr}$) associated with variable Hg isotopic composition ($\delta^{202}\text{Hg}$: -1.02‰ to -2.01‰ ; $\Delta^{199}\text{Hg}$: -0.16‰ to -0.50‰ ; $\Delta^{200}\text{Hg}$: -0.08‰ to 0.07‰). Using a $\Delta^{200}\text{Hg}$ -based model, deposition fluxes of atmospheric Hg(0) and Hg(II) were estimated, which vary coherently with climatic indices (e.g., temperature, precipitation, and monsoon intensity). Results of this study imply that atmospheric Hg deposition in SW China is governed by two climate scenarios. In warm-house climates, low precipitation intensity and vegetation growth rates in SW China caused low atmospheric Hg(II) and Hg(0) deposition fluxes, respectively. In cold-house climates, high precipitation intensity and vegetation growth rates caused high atmospheric Hg(II) and Hg(0) deposition fluxes. This study highlights that climate changes can have a strong control on atmospheric Hg deposition.

INTRODUCTION


Mercury (Hg) is a volatile and toxic heavy metal, and the atmosphere plays a vital role in the global Hg cycle (Driscoll et al., 2013). In ecosystems, Hg is readily transformed into methylmercury, a bioaccumulative neurotoxin of potent health threat to wildlife and humans (Mergler et al., 2007). The Minamata Convention on Mercury, adopted by the United Nations Environment Programme in 2013, entered into force in 2017 with the goal of reducing global anthropogenic Hg emissions. The success of this convention requires our knowledge of

atmospheric Hg emission and deposition of the past, present, and future.

Mercury is released into the atmosphere via natural and anthropogenic processes (Pirrone et al., 2010). Atmospheric Hg emission was dominated by natural processes in preindustrial periods, whereas anthropogenic processes have increased global Hg emission by a factor of three to five since global industrialization (Amos et al., 2013). Studies on sediment cores worldwide have reported elevated Hg influx in the past decades, which were attributed to anthropogenic Hg enrichments to lakes and oceans via either atmospheric deposition or soil erosion (Kang et al., 2016; Taylor et al., 2022). These studies also demonstrated dramatic changes in Hg input over preindustrial periods, but the driving forces for these variations were rarely discussed. Few studies imply that, in addition to anthropogenic

activities, climate may be an important factor governing atmospheric Hg deposition. For instance, some remote areas have shown elevated atmospheric Hg deposition due to large amounts of rain and snowfall sequestering atmospheric Hg(II) species (Dastoor et al., 2022; Jiskra et al., 2022). Atmospheric Hg(0) levels in global forests are lower in summer due to the assimilation of atmospheric Hg(0) by forests (Jiskra et al., 2018). Jitaru et al. (2009) reconstructed a 670 k.y. Hg deposition record using an ice core collected from Dome C, Antarctica, and showed greater atmospheric Hg deposition during cooler climatic stages. Yet, the Hg deposition history in the preindustrial era is poorly constrained and little is known about the relationship between Hg and climate change in non-polar regions.

Compared to lake and ocean sediments that receive a substantial amount of Hg from soil erosion, peat cores are suitable natural archives for reconstructing long-term atmospheric Hg deposition because peatlands receive Hg mainly via vegetation uptake of gaseous Hg(0) and wet deposition of atmospheric Hg(II) (Enrico et al., 2016). Mercury isotopes undergo mass-dependent fractionation (MDF, reported as $\delta^{202}\text{Hg}$) and mass-independent fractionation (MIF, reported as $\Delta^{199}\text{Hg}$, $\Delta^{200}\text{Hg}$, and $\Delta^{201}\text{Hg}$), which offer key insights into the sources and fate of Hg in the environment (Blum et al., 2014; Kwon et al., 2020). A recent study yielded a dramatic variation of peat $\Delta^{200}\text{Hg}$, which was used to quantify the relative importance of atmospheric Hg(0) and Hg(II) deposition during the Holocene (Enrico et al., 2016). Yet, the application of Hg isotopes in peat cores across low latitudes, especially in alpine areas characterized by atmospheric Hg deposition over a large regional scale, is lacking.

Runsheng Yin  <https://orcid.org/0000-0002-8072-0774>

Linchuan Fang  <https://orcid.org/0000-0003-1923-7908>
*yinrunsheng@mail.gyig.ac.cn; flinc629@hotmail.com

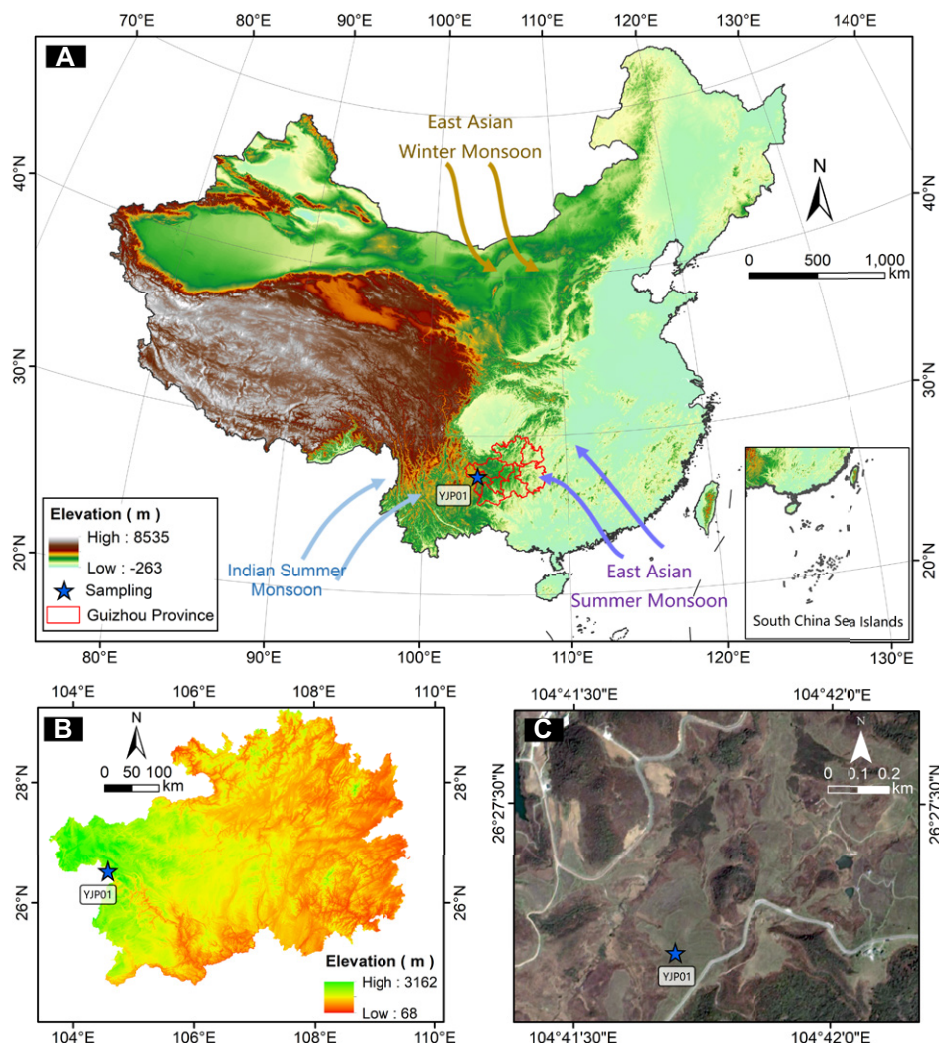


Figure 1. (A) Location of Yeiping peat bog in SW China and wind direction of East Asian summer monsoon, East Asian winter monsoon, and Indian summer monsoon. (B) Topography of Guizhou province, SW China. (C) Satellite image of sampling site.

Here, we analyze the Hg concentration and isotopic composition of a peat core taken from Yunnan-Guizhou Plateau, SW China. Combined with high-precision ^{14}C dating and paleoclimatic data in East Asia, we reconstruct a 1200-year record of Hg deposition in SW China and demonstrate that climate changes can have a strong control on atmospheric Hg deposition.

STUDY AREAS AND SAMPLES

The Yeiping peat bog ($26^{\circ}27'\text{N}$, $104^{\circ}41'\text{E}$, 2241 m above sea level) is an alpine peat bog located in Yunnan-Guizhou Plateau (Fig. 1). Its remote location precludes local anthropogenic influences. It has steep topography and lacks rivers or streams nearby. The annual precipitation is 1200 mm and the vegetation is dominated by herbaceous plants at the study location (Zhang and Wu, 2021).

A 450-cm-long peat core, YJP01, covering the past 1200 years based on accelerator mass spectrometry (AMS) ^{14}C dating, was collected from the Yeiping peat bog (Zeng et al., 2022).

The core was sliced into 1 cm sub-samples, freeze-dried, ground, and homogenized prior to chemical analysis at the Institute of Geochemistry, Chinese Academy of Sciences. Sedimentation rates of the core have been recently reported (Zeng et al., 2022).

ANALYTICAL METHODS

Total organic carbon (TOC) concentrations (Table S1 in the Supplemental Material¹) were measured following Nelson and Sommers (1996), which yielded a relative standard deviation of <5% for duplicate samples. Total Hg (THg) concentrations (Table S1) were determined using a DMA-80 Hg analyzer (Milestone, Italy), which yielded Hg recoveries of 90%–110% for GSS-5 soil standard reference material (SRM; $n = 6$) and relative standard deviations of

¹Supplemental Material. Tables S1 and S2. Please visit <https://doi.org/10.1130/GEOL.S.23647029> to access the supplemental material, and contact editing@geosociety.org with any questions.

<10% (2SD) for sample duplicates. Hg deposition influx ($\text{Hg}_{\text{influx}}$) for each time interval was calculated by multiplying sedimentation rates by THg concentrations.

Mercury isotopic composition (Table S2) was measured following Yin et al. (2016). Briefly, the samples were preconcentrated into 40% HNO_3/HCl (2/1, v/v) trapping solutions using a double-stage tube furnace. The trapping solutions were diluted to 1 ng/mL Hg with $\sim 10\%$ acidity and measured using a Neptune Plus multi-collector-inductively coupled plasma-mass spectrometer. Hg-MDF is expressed in $\delta^{202}\text{Hg}$ notation in units of per mil (‰) referenced to the NIST-3133 Hg standard:

$$\delta^{202}\text{Hg} (\text{‰}) = \left[\frac{(^{202}\text{Hg}/^{198}\text{Hg})_{\text{sample}}}{(^{202}\text{Hg}/^{198}\text{Hg})_{\text{standard}} - 1} \right] \times 1000. \quad (1)$$

Hg-MIF is reported in Δ notation, which describes the difference between the measured and the theoretically predicted δ values defined by MDF law:

$$\Delta^{\text{xxx}}\text{Hg} (\text{‰}) = \delta^{\text{xxx}}\text{Hg} - \delta^{202}\text{Hg} \times \beta, \quad (2)$$

where xxx equals 199, 200, or 201, with corresponding β values of 0.252, 0.502, or 0.752, respectively (Blum and Bergquist, 2007). GSS-4 soil SRM was prepared and measured the same way as the samples. NIST-3177 secondary Hg standard solutions (1 ng/mL Hg in 10% HCl) were measured for every 10 samples. The results of NIST-3177 ($\delta^{202}\text{Hg} = -0.52\text{‰} \pm 0.09\text{‰}$; $\Delta^{199}\text{Hg} = -0.03\text{‰} \pm 0.06\text{‰}$; $\Delta^{200}\text{Hg} = -0.01\text{‰} \pm 0.06\text{‰}$; $\Delta^{201}\text{Hg} = -0.02\text{‰} \pm 0.06\text{‰}$; 2SD, $n = 7$) and GSS-4 ($\delta^{202}\text{Hg} = -1.60\text{‰} \pm 0.07\text{‰}$; $\Delta^{199}\text{Hg} = -0.44\text{‰} \pm 0.08\text{‰}$; $\Delta^{200}\text{Hg} = -0.02\text{‰} \pm 0.08\text{‰}$; $\Delta^{201}\text{Hg} = -0.36\text{‰} \pm 0.11\text{‰}$; 2SD, $n = 4$) agree well with previous results (Blum and Bergquist, 2007; Yin et al., 2022).

RESULTS

The studied core shows a large variation of TOC (2.86–65.6 wt%; Fig. 2A), THg (62.2–302 ng/g; Fig. 2B), and $\text{Hg}_{\text{influx}}$ (30.3–515 $\mu\text{g}/\text{m}^2/\text{yr}$; Fig. 2C). This core shows consistently negative values of $\delta^{202}\text{Hg}$ (-1.02‰ to -2.01‰ ; Fig. 2F) and $\Delta^{199}\text{Hg}$ (-0.16‰ to -0.50‰ ; Fig. 2E) and variable $\Delta^{200}\text{Hg}$ (-0.08‰ to 0.07‰ ; Fig. 2D).

In the past 1200 years, East Asia experienced three climatic events (Fig. 2): the Medieval Warm Period (MWP, 1000–500 calibrated [cal] yr B.P.), the Little Ice Age (LIA, 500–100 cal. yr B.P.), and the Current Warm Period (CWP, 100 cal. yr B.P. to present) (Sun et al., 2021). Distinct patterns are shown in the three events. The MWP shows the lowest values of THg (128 ± 24.7 ng/g, SD), $\text{Hg}_{\text{influx}}$ (113 ± 80 $\mu\text{g}/\text{m}^2/\text{yr}$, SD), and TOC (19.8 ± 11.8 wt%,

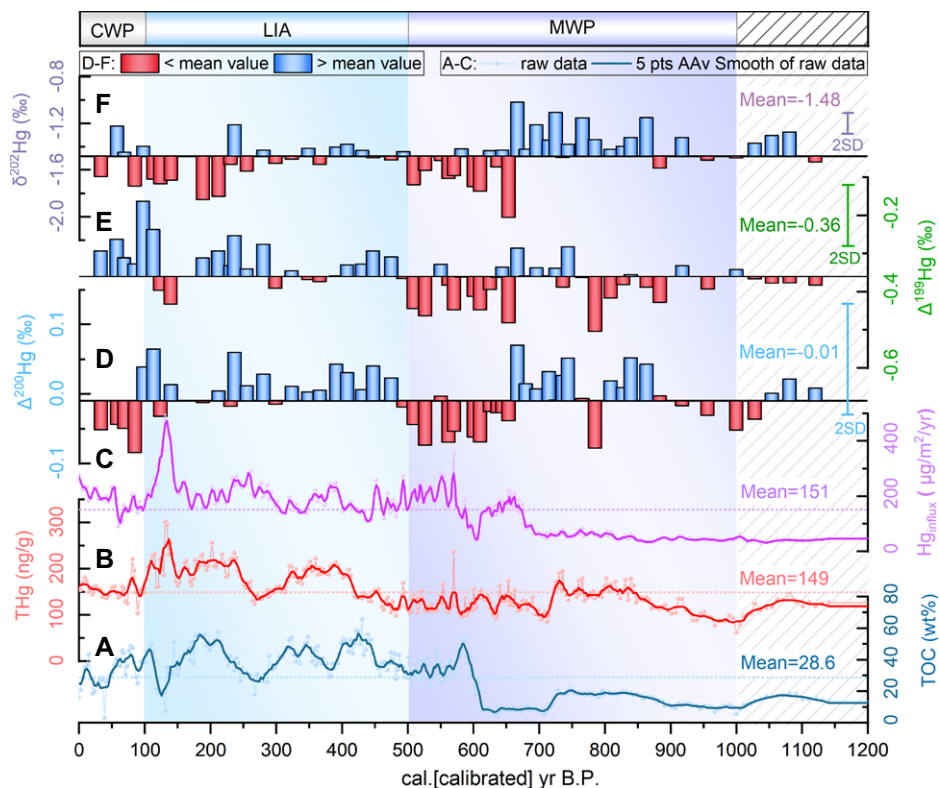


Figure 2. Total organic carbon (TOC; A), total Hg (THg; B), Hg deposition influx (Hg_{influx} ; C), $\Delta^{200}Hg$; D), $\Delta^{199}Hg$; E), and $\delta^{202}Hg$; F) in YJP01 peat core. CWP—Current Warm Period; LIA—Little Ice Age; MWP—Medieval Warm Period.

SD). The LIA shows the highest values of THg (179 ± 38.2 ng/g, SD), Hg_{influx} (214 ± 67.7 $\mu\text{g}/\text{m}^2/\text{yr}$, SD), and TOC (40.6 ± 10.0 wt%, SD). The CWP shows intermediate values of THg (155 ± 20.3 ng/g, SD), Hg_{influx} (181 ± 19.8 $\mu\text{g}/\text{m}^2/\text{yr}$, SD), and TOC (32.8 ± 9.5 wt%, SD). As for Hg isotopes, the $\delta^{202}Hg$ values are consistently negative among the MWP ($-1.46\text{‰} \pm 0.22\text{‰}$, SD), LIA ($-1.54\text{‰} \pm 0.16\text{‰}$, SD), and CWP ($-1.49\text{‰} \pm 0.21\text{‰}$, SD). The $\Delta^{199}Hg$ values show an overall increase from the MWP ($-0.38\text{‰} \pm 0.05\text{‰}$, SD) to LIA ($-0.33\text{‰} \pm 0.05\text{‰}$, SD) to CWP ($-0.27\text{‰} \pm 0.07\text{‰}$, SD). A variation of 0.15‰ in $\Delta^{200}Hg$ is observed throughout the MWP (-0.08‰ to 0.07‰), LIA (-0.03‰ to 0.06‰), and CWP (-0.08‰ to 0.04‰). It should be noted that the period ca. 650–850 yr B.P. is associated with anomalously high $\delta^{202}Hg$, $\Delta^{199}Hg$, and $\Delta^{200}Hg$ values compared to the rest of the MWP. These anomalies correspond to a slight decrease in temperature (~ 0.2 °C) in the Northern Hemisphere during the same period (Mann et al., 2009).

DISCUSSION

Limited Anthropogenic Control on Atmospheric Hg Deposition to the Studied Peat Bog

In contrast with the rapid rise of anthropogenic Hg emissions since global industrialization (Amos et al., 2013), a sharp increase in Hg

concentrations and Hg_{influx} during the CWP was not observed in the Yejiaping core (Figs. 2B and 2C). This could be due to either (1) the remote nature of the Yejiaping peat bog far away from anthropogenic Hg emission sources, or (2) the lack of a valid ^{14}C -based age model for the Yejiaping core for the past 150 years (Zeng et al., 2022). The observation of higher Hg concentrations and Hg_{influx} in the LIA samples than the CWP samples likewise suggests that natural processes, potentially induced by climate changes (discussed below), may play a more important role in introducing Hg to the biosphere.

Quantifying Wet versus Dry Hg Deposition Using Hg Isotopes

Quantifying the relative importance of atmospheric Hg dry and wet deposition pathways, which occurs in the forms of Hg(0) and Hg(II), respectively, can aid in understanding the role of climatic control on the variation of Hg concentrations and isotope ratios in the peat core. $\delta^{202}Hg$ provides a poor constraint on these two pathways because Hg-MDF occurs during various processes (Blum et al., 2014). Vegetation uptake of Hg(0) favors incorporation of lighter Hg isotopes (Yin et al., 2013), which may explain the negative $\delta^{202}Hg$ values of our samples. Vegetation uptake of Hg(0) is thought to trigger MIF in odd-mass Hg isotopes due to photoreduction of Hg(II) in leaf cells (Demers et al., 2013); therefore, $\Delta^{199}Hg$ may also not be an ideal Hg source

tracer. MIF of ^{200}Hg is thought to be generated by upper tropospheric or stratospheric photochemical reactions (Chen et al., 2012; Fu et al., 2021). Therefore, $\Delta^{200}Hg$ is considered a conservative tracer for atmospheric Hg deposition, and the variation of $\Delta^{200}Hg$ in peat cores is reflective of varying proportions of atmospheric Hg(0) and Hg(II) deposition (Enrico et al., 2017). With well-estimated mean $\Delta^{200}Hg$ values of -0.06‰ and 0.16‰ for global atmospheric Hg(0) and Hg(II) samples, respectively, the proportions of atmospheric Hg(0) and Hg(II) deposition to peatlands can be calculated using a binary mixing model, based on the $\Delta^{200}Hg$ of the peat sample (Enrico et al., 2017).

Based on the same model by Enrico et al. (2017) and the mean $\Delta^{200}Hg$ values of samples for the MWP ($-0.01\text{‰} \pm 0.04\text{‰}$, SD), LIA ($0.01\text{‰} \pm 0.03\text{‰}$, SD), and CWP ($-0.04\text{‰} \pm 0.05\text{‰}$, SD), we calculate the proportions of atmospheric Hg(0) and Hg(II) deposition during the three periods. The model outputs reveal Hg(0) proportions of $79\% \pm 19\%$ (1SD), $67\% \pm 12\%$, and $90\% \pm 21\%$ during the MWP, LIA, and CWP, respectively (Fig. 3A). The estimated Hg(II) proportions are $21\% \pm 19\%$, $33\% \pm 12\%$, and $10\% \pm 21\%$, respectively. By multiplying Hg_{influx} by the estimated proportions, Hg_{influx} of atmospheric Hg(0) and Hg(II), termed $Hg_{influx-Hg(0)}$ and $Hg_{influx-Hg(II)}$, respectively, was calculated (Fig. 3B). The estimated $Hg_{influx-Hg(0)}$ values are 93.2 ± 77.5 $\mu\text{g}/\text{m}^2/\text{yr}$ (SD), 144 ± 58.2 $\mu\text{g}/\text{m}^2/\text{yr}$ (SD) and 166 ± 50.9 $\mu\text{g}/\text{m}^2/\text{yr}$ (SD) during the MWP, LIA, and CWP, respectively. The estimated $Hg_{influx-Hg(II)}$ values are 19.4 ± 21.3 $\mu\text{g}/\text{m}^2/\text{yr}$ (SD), 70 ± 33.1 $\mu\text{g}/\text{m}^2/\text{yr}$ (SD) and 15.3 ± 33.3 $\mu\text{g}/\text{m}^2/\text{yr}$ (SD) during the MWP, LIA, and CWP, respectively. Overall, we find that on a temporal scale, the CWP reflects the highest proportion of Hg(0) deposition and the LIA reflects the highest proportion of Hg(II) deposition. No $Hg_{influx-Hg(II)}$ and $Hg_{influx-Hg(0)}$ anomalies are shown during 650–850 yr B.P. compared to the rest of the MWP (Fig. 3B), suggesting that the previously reported slight decrease in temperature during this period (Mann et al., 2009) was of little importance to the changing of atmospheric Hg deposition pattern during the MWP.

Climatic Change as a Dominant Control on Atmospheric Hg Deposition

To identify the potential climatic control on atmospheric Hg deposition in the Yejiaping peat bog, we compared our results with available climate data in East Asia, including annual temperatures in SW China (Fig. 3F), the East Asian summer monsoon (EASM) and East Asian winter monsoon (EAWM) indexes (Figs. 3C and 3E), and the Southern Oscillation index (SOI; Fig. 3D). Clearly, the LIA had consistently higher $Hg_{influx-Hg(II)}$, lower EASM intensities, higher EAWM intensities, and lower tempera-

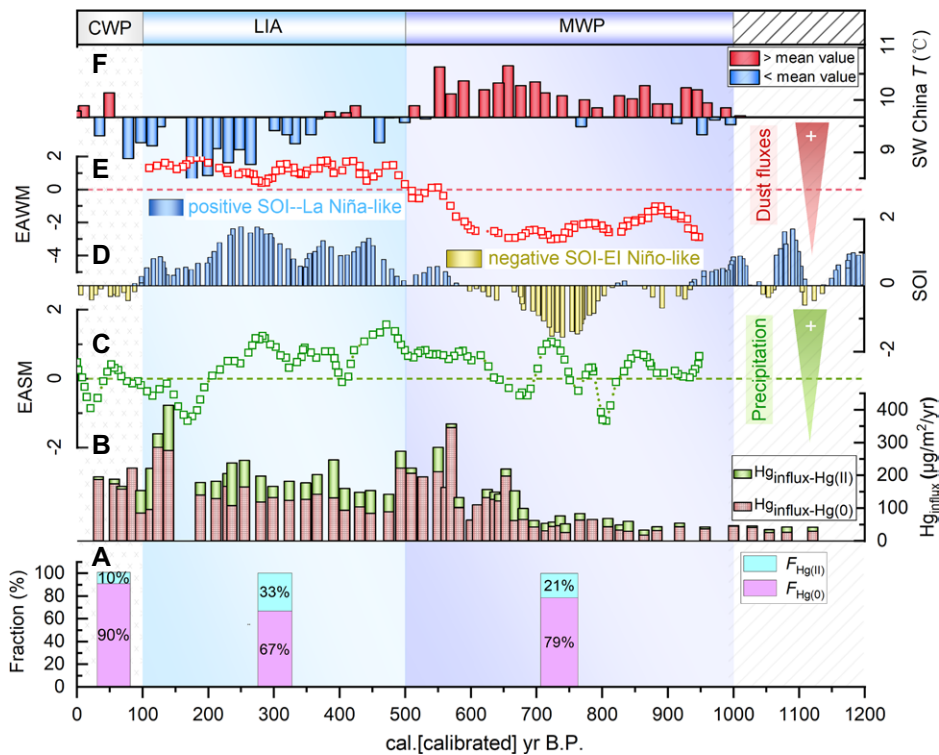


Figure 3. (A) Fractions (F) of atmospheric Hg(0) deposition and Hg(II) deposition. (B) Hg deposition influx of atmospheric Hg(0) and Hg(II) ($Hg_{influx-Hg(0)}$ and $Hg_{influx-Hg(II)}$) respectively. (C, E) East Asian summer monsoon (EASM) index (C) and East Asian winter monsoon (EAWM) index (E) (Hu et al., 2022). (D) Southern Oscillation index (SOI; Yan et al., 2011). (F) Reconstructed annual temperature (T) of SW China (Yan et al., 2020). CWP—Current Warm Period; LIA—Little Ice Age; MWP—Medieval Warm Period.

tures relative to other periods. The EAWM and EASM are two dominant monsoons governing the climate of East Asia, and their intensities are governed by temperatures (Hu et al., 2022). During the LIA, lower temperatures in East Asia led to enhanced EAWM and weakened EASM (Hu et al., 2022), resulting in a southward migration of rainfall (supported by more positive SOI values). This would have increased the amount of precipitation in SW China (Liu et al., 2022), resulting in wet Hg(II) deposition and therefore the enhanced $Hg_{influx-Hg(II)}$ during the LIA. Conversely, an increase in temperature and a northward movement of rainfall and low rainfall rates in SW China would explain the lower $Hg_{influx-Hg(II)}$ during the MWP.

Increased precipitation during the LIA may also have indirectly increased the magnitude of Hg(0) uptake through promoting vegetative growth or altering the vegetation species of the peatland (Rydberg et al., 2010), which explains the higher degree of $Hg_{influx-Hg(0)}$ during this period than the MWP. Enhanced vegetative growth seems to be supported by the highest TOC levels during the LIA, although the TOC content may not fully represent the biomass of the peat bog due to organic matter decomposition during burial (Nieminen et al., 2021). Conversely, low rainfall rates in SW China would have resulted in changes in vegetation species and low vegetation growth and therefore low

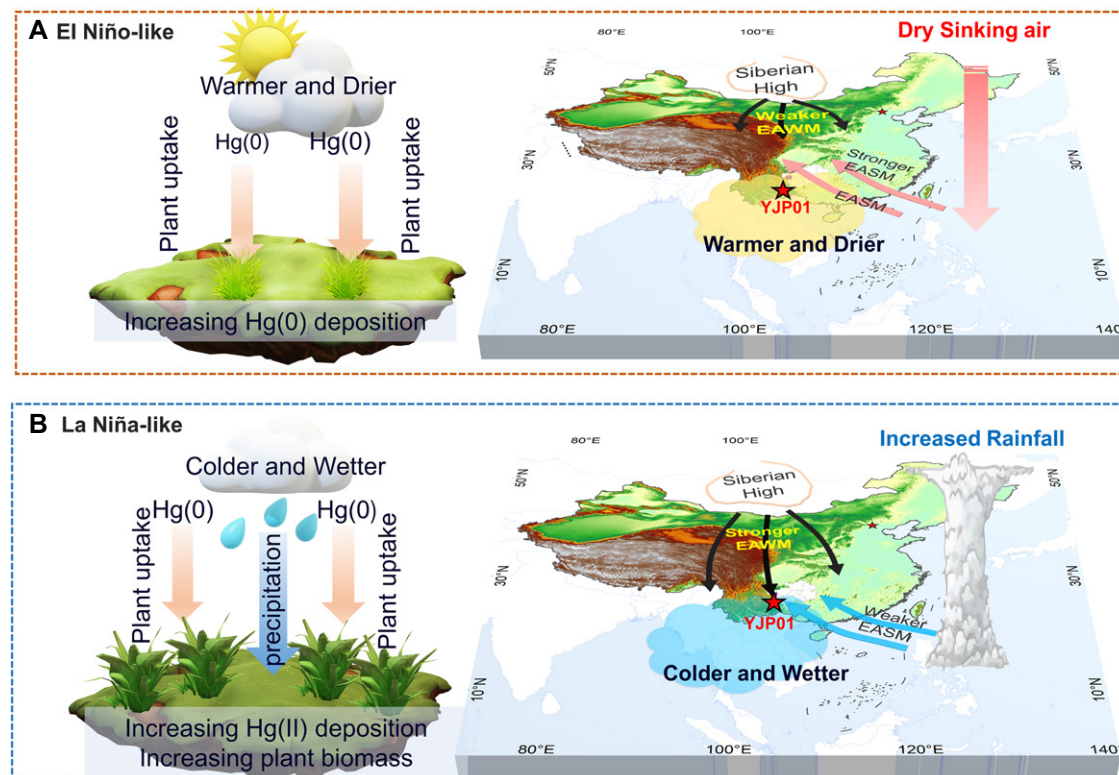


Figure 4. Schematic diagram showing two contrasting modes of atmospheric Hg deposition in SW China. (A) In El Niño-like climate, weakened East Asian winter monsoon (EAWM) resulted in dry sinking air, low precipitation and vegetation growth, and low Hg deposition influx of atmospheric Hg(0) and Hg(II) [$Hg_{influx-Hg(0)}$ and $Hg_{influx-Hg(II)}$] respectively in SW China. (B) In La Niña-like climate, enhanced EAWM resulted in more rainfall and vegetation growth and high $Hg_{influx-Hg(0)}$ and $Hg_{influx-Hg(II)}$ in SW China (Hu et al., 2022; Liu et al., 2022). EASM—East Asian summer monsoon.

Hg_{influx-Hg(0)} during MWP. An increase in Hg_{influx-Hg(0)} in the CWP may be explained by vegetation uptake of atmospheric Hg(0) that has been increased by a factor of three to five due to rapid anthropogenic Hg emission during this period (Amos et al., 2013).

CONCLUSIONS AND IMPLICATIONS

This study provides evidence of climatic control on atmospheric Hg deposition and proposes two contrasting modes of atmospheric Hg deposition in SW China. In the first mode (Fig. 4A), such as that presented in the MWP and CWP, SW China was in an El Niño-like (warm-house) climate, which is not conducive to atmospheric Hg deposition due to low rainfall rates and low vegetation growth rates. In the second mode (Fig. 4B), such as that presented in the LIA, SW China experienced a La Niña-like (cool-house) climate that favored atmospheric Hg deposition due to high rainfall rates and high vegetation growth rates. This study, therefore, sheds new light on understanding past and future atmospheric Hg deposition driven by climate changes.

ACKNOWLEDGMENTS

This study is supported by the Chinese Academy of Sciences through Hundred Talent Plan and the Strategic Priority Research Program (XDB40020202).

REFERENCES CITED

Amos, H.M., Jacob, D.J., Streets, D.G., and Sunderland, E.M., 2013, Legacy impacts of all-time anthropogenic emissions on the global mercury cycle: Global Biogeochemical Cycles, v. 27, p. 410–421, <https://doi.org/10.1002/gbc.20040>.

Blum, J.D., and Bergquist, B.A., 2007, Reporting of variations in the natural isotopic composition of mercury: Analytical and Bioanalytical Chemistry, v. 388, p. 353–359, <https://doi.org/10.1007/s00216-007-1236-9>.

Blum, J.D., Sherman, L.S., and Johnson, M.W., 2014, Mercury isotopes in earth and environmental sciences: Annual Review of Earth and Planetary Sciences, v. 42, p. 249–269, <https://doi.org/10.1146/annurev-earth-050212-124107>.

Chen, J.B., Hintelmann, H., Feng, X.B., and Dimock, B., 2012, Unusual fractionation of both odd and even mercury isotopes in precipitation from Peterborough, ON, Canada: Geochimica et Cosmochimica Acta, v. 90, p. 33–46, <https://doi.org/10.1016/j.gca.2012.05.005>.

Dastoor, A., et al., 2022, Arctic mercury cycling: Nature Reviews Earth & Environment, v. 3, p. 270–286, <https://doi.org/10.1038/s43017-022-00269-w>.

Demers, J.D., Blum, J.D., and Zak, D.R., 2013, Mercury isotopes in a forested ecosystem: Implications for air-surface exchange dynamics and the global mercury cycle: Global Biogeochemical Cycles, v. 27, p. 222–238, <https://doi.org/10.1002/gbc.20021>.

Driscoll, C.T., Mason, R.P., Chan, H.M., Jacob, D.J., and Pirrone, N., 2013, Mercury as a global pollutant: Sources, pathways, and effects: Environmental Science & Technology, v. 47, p. 4967–4983, <https://doi.org/10.1021/es305071v>.

Enrico, M., Le Roux, G., Maruszczak, N., Heimbürger, L.-E., Claustres, A., Fu, X.W., Sun, R.Y., and Sonke, J.E., 2016, Atmospheric mercury transfer to peat bogs dominated by gaseous elemental

mercury dry deposition: Environmental Science & Technology, v. 50, p. 2405–2412, <https://doi.org/10.1021/acs.est.5b06058>.

Enrico, M., Le Roux, G., Heimbürger, L.-E., Van Beek, P., Souhaut, M., Chmeleff, J., and Sonke, J.E., 2017, Holocene atmospheric mercury levels reconstructed from peat bog mercury stable isotopes: Environmental Science & Technology, v. 51, no. 11, p. 5899–5906, <https://doi.org/10.1021/acs.est.6b05804>.

Fu, X.W., Jiskra, M., Yang, X., Maruszczak, N., Enrico, M., Chmeleff, J., Heimbürger-Boavida, L.-E., Gheusi, F., and Sonke, J.E., 2021, Mass-independent fractionation of even and odd mercury isotopes during atmospheric mercury redox reactions: Environmental Science & Technology, v. 55, p. 10,164–10,174, <https://doi.org/10.1021/acs.est.1c02568>.

Hu, F.G., Li, Y.C., Liang, J., Li, Z.Z., Xie, M.Z., Chen, X.L., and Xiao, Z.C., 2022, History of coastal dune evolution in the Fujian region of southeastern China over the last millenium: Marine Geology, v. 451, <https://doi.org/10.1016/j.margeo.2022.106878>.

Jiskra, M., et al., 2018, A vegetation control on seasonal variations in global atmospheric mercury concentrations: Nature Geoscience, v. 11, p. 244–250, <https://doi.org/10.1038/s41561-018-0078-8>.

Jiskra, M., Guédron, S., Tolu, J., Fritz, S.C., Baker, P.A., and Sonke, J.E., 2022, Climatic controls on a Holocene mercury stable isotope sediment record of Lake Titicaca: ACS Earth and Space Chemistry, v. 6, p. 346–357, <https://doi.org/10.1021/acsearthspacechem.1c00304>.

Jitaru, P., Gabrielli, P., Marteel, A., Plane, J.M.C., Planchon, F.A.M., Gauchard, P.A., Ferrari, C.P., Boutroun, C.F., Adams, F.C., and Hong, S., 2009, Atmospheric depletion of mercury over Antarctica during glacial periods: Nature Geoscience, v. 2, no. 7, p. 505–508, <https://doi.org/10.1038/ngeo549>.

Kang, S.C., et al., 2016, Atmospheric mercury depositional chronology reconstructed from lake sediments and ice core in the Himalayas and Tibetan Plateau: Environmental Science & Technology, v. 50, p. 2859–2869, <https://doi.org/10.1021/acs.est.5b04172>.

Kwon, S.Y., Blum, J.D., Yin, R.S., Tsui, M.T.-K., Yang, Y.H., and Choi, J.W., 2020, Mercury stable isotopes for monitoring the effectiveness of the Minamata Convention on Mercury: Earth-Science Reviews, v. 203, <https://doi.org/10.1016/j.earscirev.2020.103111>.

Liu, B., Sheng, E.G., Yu, K.K., Zhou, K.E., and Lan, J.H., 2022, Variations in monsoon precipitation over southwest China during the last 1500 years and possible driving forces: Science China Earth Sciences, v. 65, p. 949–965, <https://doi.org/10.1007/s11430-021-9888-y>.

Mann, M.E., Zhang, Z.H., Rutherford, S., Bradley, R.S., Hughes, M.K., Shindell, D., Ammann, C., Faluvegi, G., and Ni, F.B., 2009, Global signatures and dynamical origins of the Little Ice Age and Medieval Climate Anomaly: Science, v. 326, p. 1256–1260, <https://doi.org/10.1126/science.1177303>.

Mergler, D., Anderson, H.A., Chan, L.H.M., Mahaffey, K.R., Murray, M., Sakamoto, M., and Stern, A.H., 2007, Methylmercury exposure and health effects in humans: A worldwide concern: Ambio, v. 36, p. 3–11, [https://doi.org/10.1579/0044-7447\(2007\)36\[3:MEAHEI\]2.0.CO;2](https://doi.org/10.1579/0044-7447(2007)36[3:MEAHEI]2.0.CO;2).

Nelson, D.W., and Sommers, L.E., 1996, Total carbon, organic carbon, and organic matter, in Sparks, D.L., Page, A.L., Helmke, P.A., and Loepfert, R.H., eds., Methods of Soil Analysis Part 3—Chemical Methods: Madison, Wisconsin, Soil

Science Society of America, American Society of Agronomy, p. 961–1010, <https://doi.org/10.2136/sssabookser5.3>.

Nieminen, M., Sarkkola, S., Sallantausta, T., Hasselquist, E.M., and Laudon, H., 2021, Peatland drainage—A missing link behind increasing TOC concentrations in waters from high latitude forest catchments?: Science of the Total Environment, v. 774, <https://doi.org/10.1016/j.scitotenv.2021.145150>.

Pirrone, N., et al., 2010, Global mercury emissions to the atmosphere from anthropogenic and natural sources: Atmospheric Chemistry and Physics, v. 10, p. 5951–5964, <https://doi.org/10.5194/acp-10-5951-2010>.

Rydberg, J., Karlsson, J., Nyman, R., Wanhatalo, I., Näthe, K., and Bindler, R., 2010, Importance of vegetation type for mercury sequestration in the northern Swedish mire, Rödmosamyran: Geochimica et Cosmochimica Acta, v. 74, p. 7116–7126, <https://doi.org/10.1016/j.gca.2010.09.026>.

Sun, J., Ma, C.M., Zhou, B., Jiang, J.W., and Zhao, C., 2021, Biogeochemical evidence for environmental and vegetation changes in peatlands from the middle Yangtze river catchment during the medieval warm period and little ice Age: The Holocene, v. 31, p. 1571–1581, <https://doi.org/10.1177/09596836211025966>.

Taylor, V.F., Landis, J.D., and Janssen, S.E., 2022, Tracing the sources and depositional history of mercury to coastal northeastern U.S. lakes: Environmental Science: Processes & Impacts, v. 24, p. 1805–1820, <https://doi.org/10.1039/D2EM00214K>.

Yan, D.N., Xu, H., Lan, J.H., Yang, M., Wang, F.S., Hou, W.G., Zhou, K.G., and An, Z.S., 2020, Warming favors subtropical lake cyanobacterial biomass increasing: Science of the Total Environment, v. 726, <https://doi.org/10.1016/j.scitotenv.2020.138606>.

Yan, H., Sun, L.G., Wang, Y.H., Huang, W., Qiu, S.C., and Yang, C.Y., 2011, A record of the Southern Oscillation Index for the past 2,000 years from precipitation proxies: Nature Geoscience, v. 4, p. 611–614, <https://doi.org/10.1038/ngeo1231>.

Yin, R., Krabbenhoft, D.P., Bergquist, B.A., Zheng, W., Lepak, R.F., and Hurley, J.P., 2016, Effects of mercury and thallium concentrations on high precision determination of mercury isotopic composition by Neptune Plus multiple collector inductively coupled plasma mass spectrometry: Journal of Analytical Atomic Spectrometry, v. 31, no. 10, p. 2060–2068, <https://doi.org/10.1039/c6ja00107f>.

Yin, R.S., Feng, X.B., and Meng, B., 2013, Stable mercury isotope variation in rice plants (*Oryza sativa* L.) from the Wanshan mercury mining district, SW China: Environmental Science & Technology, v. 47, p. 2238–2245, <https://doi.org/10.1021/es304302a>.

Yin, R.S., et al., 2022, Mantle Hg isotopic heterogeneity and evidence of oceanic Hg recycling into the mantle: Nature Communications, v. 13, 948, <https://doi.org/10.1038/s41467-022-28577-1>.

Zeng, M.X., Zeng, Q., Peng, H.J., Wu, Y.Q., Li, Y., Song, Y.G., Sheng, E.G., Wu, Y.Y., Wang, T.Y., and Ni, J., 2022, Late Holocene hydroclimatic changes inferred from a karst peat archive in the western Guizhou Plateau, SW China: Journal of Asian Earth Sciences, v. 229, <https://doi.org/10.1016/j.jseae.2022.105179>.

Zhang, C., and Wu, S.H., 2021, An analysis on moisture source of extreme precipitation in Southwest China in summer: Journal of Natural Resources, v. 36, p. 1186–1194, <https://doi.org/10.31497/zrzyxb.20210508> (in Chinese with English abstract).

Printed in the USA